LA-UR- 10-04375

Title: Weld Solidification Cracking in 304 to 304L Stainless Steel

Author(s): Patrick Hochanadel, Thomas Lienert, Raymond Martinez, Jesse Martinez and Matthew Johnson

Intended for: Conference Proceedings for the 3rd International Hot Cracking Workshop (DRAFT FOR PEER REVIEW)
March 15-16, 2010
Columbus, Ohio, USA

Los Alamos
NATIONAL LABORATORY
EST. 1943

Weld Solidification Cracking in 304 to 304L Stainless Steel

P.W. Hochanadel, T.J. Lienert, J.N. Martinez, R.J. Martinez and M.Q. Johnson

Los Alamos National Laboratory, Los Alamos, New Mexico USA

Abstract

A series of annulus welds were made between 304 and 304L stainless steel coaxial tubes using both pulsed laser beam welding (LBW) and pulsed gas tungsten arc welding (GTAW). In this application, a change in process from pulsed LBW to pulsed gas tungsten arc welding was proposed to limit the possibility of weld solidification cracking since weldability diagrams developed for GTAW display a greater range of compositions that are not crack susceptible relative to those developed for pulsed LBW. Contrary to the predictions of the GTAW weldability diagram, cracking was found.This result was rationalized in terms of the more rapid solidification rate of the pulsed gas tungsten arc welds. In addition, for the pulsed LBW conditions, the material compositions were predicted to be, by themselves, "weldable" according to the pulsed LBW weldability diagram. However, the composition range along the tie line connecting the two compositions passed through the crack susceptible range. Microstructurally, the primary solidification mode (PSM) of the material processed with higher power LBW was determined to be austenite (A), while solidification mode of the materials processed with lower power LBW apparently exhibited a dual PSM of both austenite (A) and ferrite-austenite (FA) within the same weld. The materials processed by pulsed GTAW showed mostly primary austenite solidification, with some regions of either primary austenite-second phase ferrite (AF) solidification or primary ferrite-second phase austenite (FA) solidification. This work demonstrates that variations in crack susceptibility may be realized when welding different heats of "weldable" materials together, and that slight variations in processing can also contribute to crack susceptibility.

Introduction

The fact that austenitic stainless steels may be susceptible to weld solidification cracking is not new. In fact, correlations between cracking susceptibility and both the primary solidification mode (PSM) and the impurity content of these alloys have been made for a number of years [1-15]. These investigations have shown that with sufficient specific impurities and primary solidification of austenite, the weld metal is susceptible to weld solidification cracking.

In addition, constitution diagrams, such as the Schaeffler Diagram and the Welding Research Council (WRC) diagrams have been used to select filler metals and/or predict resulting weld metal constituents in stainless steel welds [16-19]. These constitution diagrams and weld cracking susceptibility diagrams are specific to welding conditions, such as cooling rate. Many investigators have shown that the primary solidification mode changes with changes in cooling rate [20-23.]. It is still convenient, however, to refer to weldability diagrams as the arc welding or pulsed laser beam welding (LBW) weldability diagram, without considering potential variations in solidification within each category. Littlework, however, has been done in documenting weld cracking susceptibility in "similar alloy", dissimilar heat austenitic stainless steel welds [23-24]. Hochanadel, *et al.*, [24] have shown that weldability diagrams may be used to analyze the weldability of two "similar" dissimilar materials by noting the composition end-points and utilizing a tie-line between the two points. In changing an existing process from pulsed LBW to pulsed GTAW, the weldability is typically expected to be improved in that the "no cracking" region of the weldability diagram is expanded in the GTAW case. This work was done to investigate the weldability response of welding two dissimilar austenitic stainless steel heats together and comparing the response when welding with both a pulsed LBW and pulsed GTAW.

Procedure

Several annulus welds were made between 304L (outer tube) and 304 (inner tube) materials with both pulsed LBW and pulsed GTAW. Figure 1 shows the top view of tubes prior to welding. The 304L outer tube was machined from bar stock and the 304 inner tube was seamless tube material. Table I lists the nominal chemical composition of the materials investigated.

A Lumonics JK706 Nd:YAG pulsed laser welder was used to make the laser welds. The average welding power ranged from 35 watts to 110 watts (verified by a "hockey-puck" or "lollipop" calorimeter), and the pulse widths investigated were either 3ms or 5ms, giving a duty cycle of 3 percent or 5 percent, since the pulse frequency was held constant at 10 Hz. The travel speed was held constant at 0.5 mm/s, and the beam diameter was approximately 1 mm. All laser welds were made at sharp visual focus.

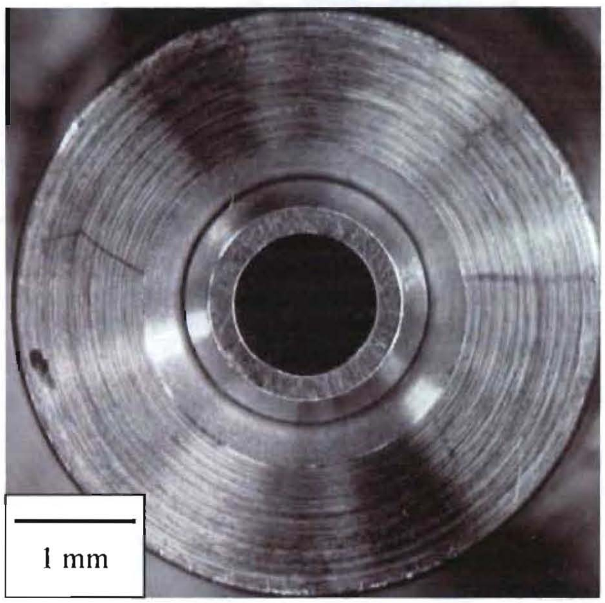

Fig. 1. Top view of the tubes prior to welding.

The pulsed GTA welds were made using an Arc Machines, Incorporated (AMI) 307 power supply/controller using a special weld head capable of performing a tube-to-tube annulus weld (see Figure 2). The weld was made with a 4 level weld and Table II lists the pulsing parameters used. The arc gap was at approximately 0.4 mm using a 1mm diameter electrode with an 18° grind angle and the tip diameter was 0.25 mm. The travel speed was approximately 4.5 mm/second.

Leak checking of the welds was performed with an Alcatel ASM 180t leak detector. Subsequent microstructural observation was performed after sectioning and polishing using standard metallographic procedures. Electrolytic etching was performed with a 10 pct. oxalic acid solution.

Table I. Nominal alloy compositions (in weight percent). Add Cr/Ni eq and % P+S

	Outer Tube (304L)	Inner Tube (304)
Cr	18.5	19.9
Ni	11.6	10.0
Mn	1.6	1.8
Si	0.36	0.46
Co	0.025	N/A
Mo	0.044	N/A
C	0.027	0.051
S	0.002	0.016
P	0.010	0.020
N	0.037	N/A
Hammar and Svensson Cr_{eq}/Ni_{eq}	1.44	1.72
S+P	0.012	0.036

Fig. 2. Specialized annulus tube weld head for use with AMI 307 welding power supply.

Table II. Pulsed Gas Tungsten Arc Welding Parameters Used in this Investigation

Level	Level Time (sec.)	Primary Current (A) Note: Pulse Duration is 0.08 sec.	Background Current (A) Note: Pulse Duration is 0.03 sec.
1	1.8	28.0	8.4
2	1.8	27.7	8.3
3	1.8	27.3	8.2
4	1.8	27.0	8.1

Note: Primary pulse duration is 0.08 second and the background pulse duration is 0.03 second.

Results and Discussion

Figure 3 shows the top views of the pulsed LBW (Figure 3a) and the pulsed GTAW (Figure 3b), while Figure 4 shows a cross-section of a typical pulsed LBW processed weld with the original tube configurations shown for comparison. Solidification cracking was observed in the cross-sections of many of the arc and laser welds.

Laser Welds

The higher power pulsed laser welds (at approximately 90 watts average power or higher) were found to be susceptible to weld solidification cracking, as shown in Figure 5. Although many of the cracks were found to be in the final weld pulse, cracks were found throughout the weld.

Normal welding conditions dictate that the top both tubes are flush. A cross-section of this condition is seen in Figure 6. In one of the off-normal conditions, the tube-to-tube offset was moved from zero (*i.e.*, flush tubes, as seen in Figure 6) to 0.25 mm (in Figure 7). This figure shows weld solidification cracking, and the average weld metal composition was estimated to be at approximately 30 percent outer tube/70 percent inner tube based upon area fraction analysis.

In the previous investigation [24], the resulting lower power welds showed a dual solidification mode (solidification as both primary austenite on one side and primary ferrite on the other, as seen in the micrograph) in the 304 to 304L weld joint, as shown in Figure 8. Figure 8 shows how epitaxial growth of primary austenite occurred initially upon solidification for a short distance, until the solidification mode shifted to primary ferrite (both in the root in Figure 8a and along the fusion boundary in 8b). This phenomena was also observed by Lippold when pulsed laser welding

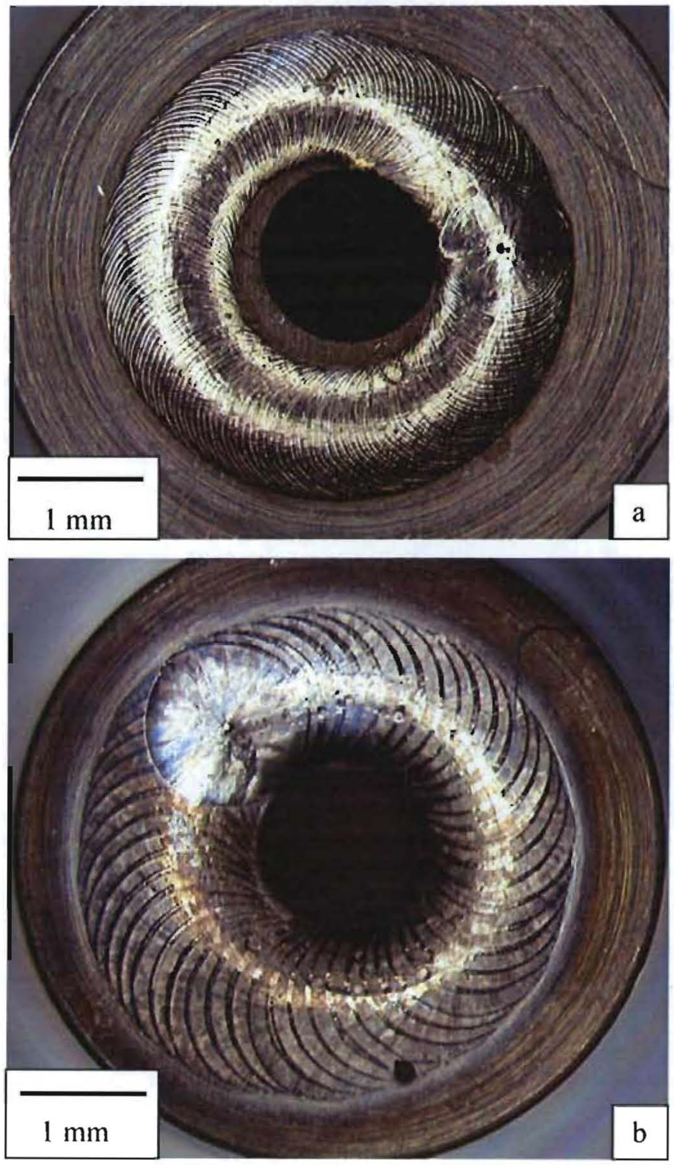

Fig. 3. Top view of the tubes after welding. The pulsed laser beam welded tubes are in 3a and the pulsed gas tungsten arc welded tubes are in 3b.

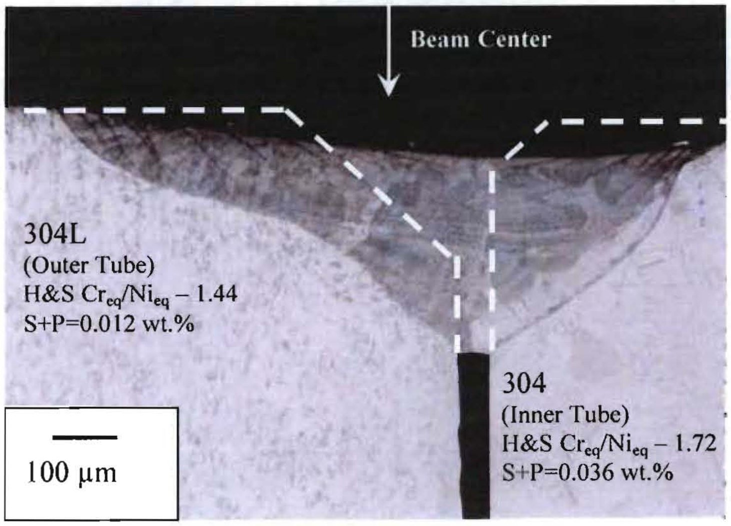

Fig. 4. Cross-section of weldment and joint schematic (dashed lines) of the 304 to 304L stainless steel combination. Average power of the weld was 45 watts and the pulse width was 5ms.

austenitic stainless steels [8], and he suggested that the diffusion controlled transformation of austenite to ferrite in the heat affected zone was suppressed, allowing for epitaxial growth of austenite. Figure 8 also shows how the solidification mode transitioned back to primary austenite, as depicted by the "A" on the right-hand side of the micrographs. This could be caused by either a change in solidification growth rate, a change in composition (as expected), or a combination of both (pulse boundary).

Figure 9 shows the fusion zone in the higher power weld. It appears that this higher power weld had only a primary solidification mode of austenite or austenite/eutectic ferrite (no evidence for primary ferrite solidification was observed). In the higher power welds (greater than 75 watts average power with 5ms pulse), the welds were found to be keyhole mode welds, while at powers lower than 75 watts, conduction mode welds were observed. Possible causes for the different solidification mode observations were either the difference in cooling rates between the two weld modes (conduction mode versus keyhole mode), the difference in mixing, or a combination of both.

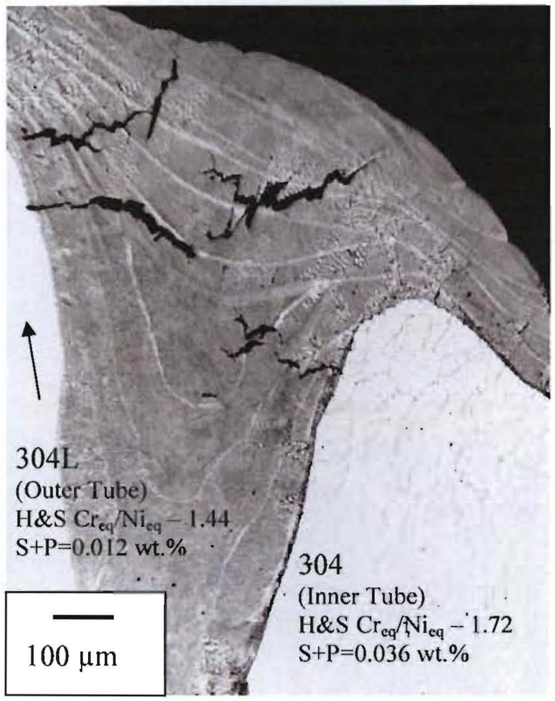

Fig. 5. Weld Solidification cracking along solidification grain boundaries in a higher power laser weld (95 watts average power and 3 ms pulse width).

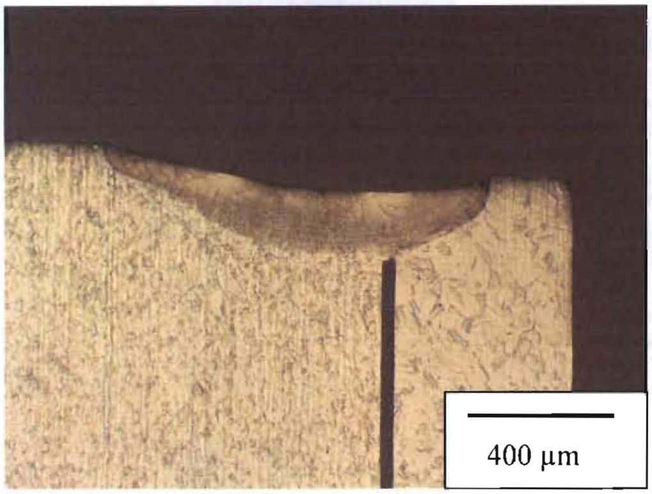

Fig. 6. Cross-section of the shallow penetration pulsed laser beam weld at nominal conditions (60 W average power, 5 ms pulse width, 10 Hz).

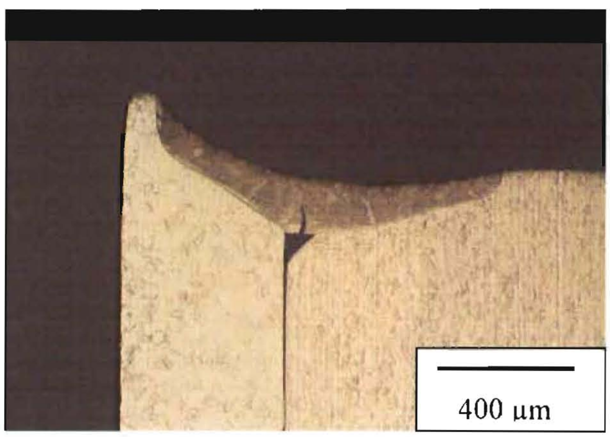

Fig. 7. Cross-section of the shallow penetration pulsed laser beam weld with a 0.25-mm tube offset (60W, 5 ms pulse width, 10Hz).

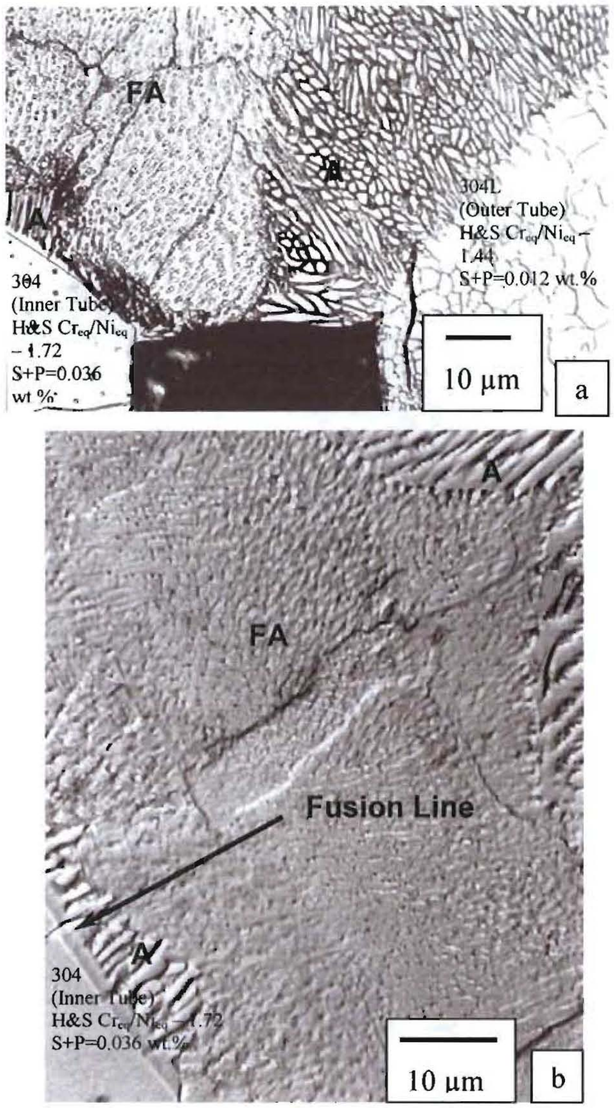

Fig. 8. Results from previous investigation showing dual primary solidification mode in the conduction mode pulsed laser beam weld. Micrograph depicting the variation in solidification microstructure at the root of the weld (8a). Fusion boundary region depicting the heat affected zone, unmixed zone and transition regions (8b). Adjacent regions of primary austenite (A) and primary ferrite (F) solidification are seen in a lower power weld (45 W average power and 5ms pulse width).

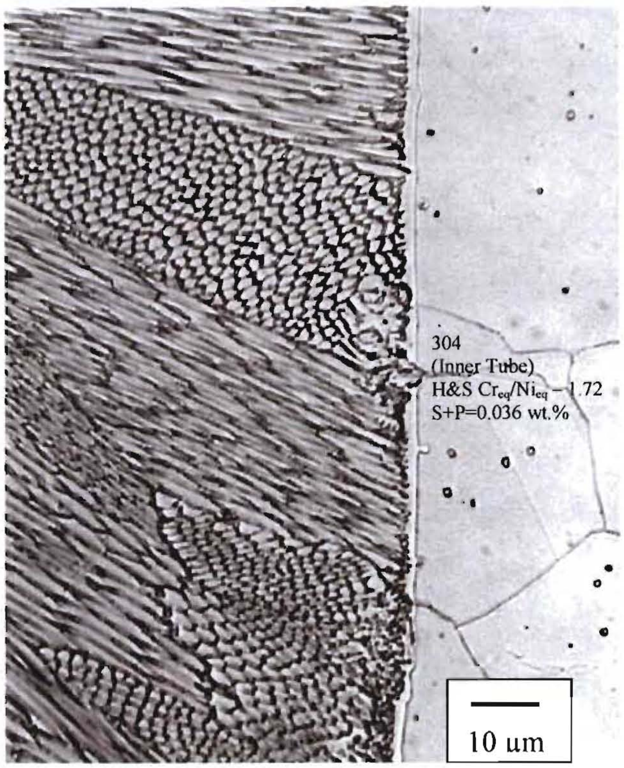

Fig. 9. Fusion zone in a higher power laser weld (95 W average power and 3 ms pulse width) showing epitaxial growth and primary austenite solidification along the high Cr_{eq}/Ni_{eq} boundary of the inner tube.

Arc Welds

A series of arc welds were also made for comparison. Figure 10 shows a cross-section of an arc weld made at nominal weld parameters and with the tubes flush to one another. Weld solidification cracking was observed in many of the arc welded materials. Note in Figure 10a how much of the weld metal appears to have a PSM of A, even though the cross-section is a low magnification. In addition, a dual primary solidification mode was observed, which was similar to some of the observations of the laser welded materials. This is shown in Figure 10b. The FA region shown in is in the region of the inner tube material – the material with the Hammar and Svensson $Cr_{eq}/Ni/_{eq}$ of 1.72.

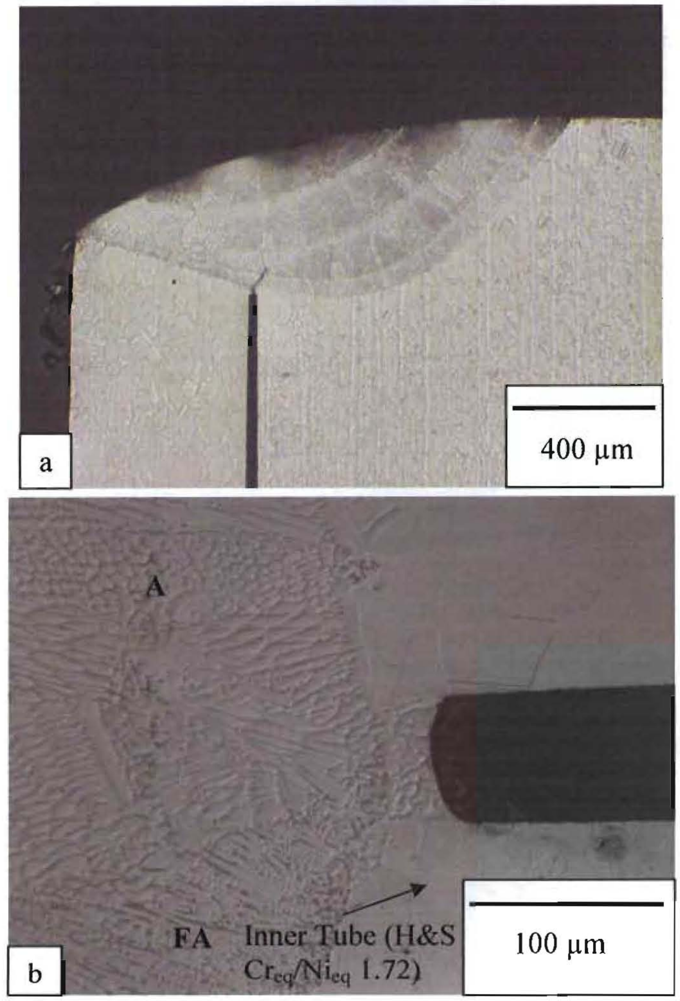

Fig. 10. Cross-section of GTAW processed materials showing weld solidification cracking in (a) and variable PSM in (b).

Discussion

By plotting the compositional window of the 304 or 304L stainless steels on the WRC 1992 constitution diagram, it is easily seen that several resulting solidification microstructures may be realized depending upon the material compositions and the extent of mixing/dilution. This is seen in Figure 11. This figure also shows the compositions of interest plotted for comparison. The WRC constitution diagram predicts that the combination of these two materials should solidify as delta ferrite and would not be expected to experience solidification cracking.

The weldability diagram modified by Lienert and Lippold to display cracking tendencies in pulsed laser welded materials is shown in Figure 12 [15]. The two compositions investigated in the current study are plotted as the Hammar and Svensson Cr_{eq}/Ni_{eq} versus the total weight % (S + P). This diagram shows clearly that both materials are readily weldable if they are laser welded autogenously. However, by placing a tie line between the two compositions, a region is found where the combination of these materials can yield a crack susceptible composition. In fact, when looking at the original weld joint configuration, an average composition of the weld metal may be calculated based upon area fraction analysis compared to the original joint configuration. It should be noted that the average weld metal composition does not necessarily represent local conditions were compositional variations are known to occur. In the case of the shallow penetration pulsed laser weld, found in Figure 6, it is seen that the average weld metal composition was found to be approximately 70 percent outer tube/30 percent inner tube. This average composition is shown as a red star on Figure 12. It is seen with no tube-to-tube offset, the average weld metal composition is in a region that borders the crack susceptibility region. Similarly, the example of tube offset of 0.25 mm (Figure 7) shows that the average composition in a region in which solidification cracking is possible (and apparent, in this case). Recall that solidification cracking is both metallurgical and mechanical - the tube offset allows sufficient mechanical driver for solidification cracking was present which may cause cracking.

It was believed that changing the welding process from pulsed LBW to pulsed GTAW would be beneficial, since the demarcation line in the weldability diagram moves from a Hammar and Svensson Cr_{eq}/Ni_{eq} of nearly 1.6 ("Solidification cracking likely") or 1.7 ("Solidification cracking possible") in the pulsed LBW weldability diagram seen in Figure 12 [15] to approximately 1.5 in the original GTAW weldability diagram [2], which is shown in Figure 13. Based upon the original joint, the average weld metal composition was estimated to be nearly 50 percent outer tube/50 percent inner tube (area fraction analysis *versus* the original joint). The composition end points and tie-line, along with the 50/50 average composition point is shown in Figure 13. Based upon this diagram, the combination of the materials should be weldable over the entire range of compositions possible. However, as seen in Figure 10, weld solidification cracking was possible.

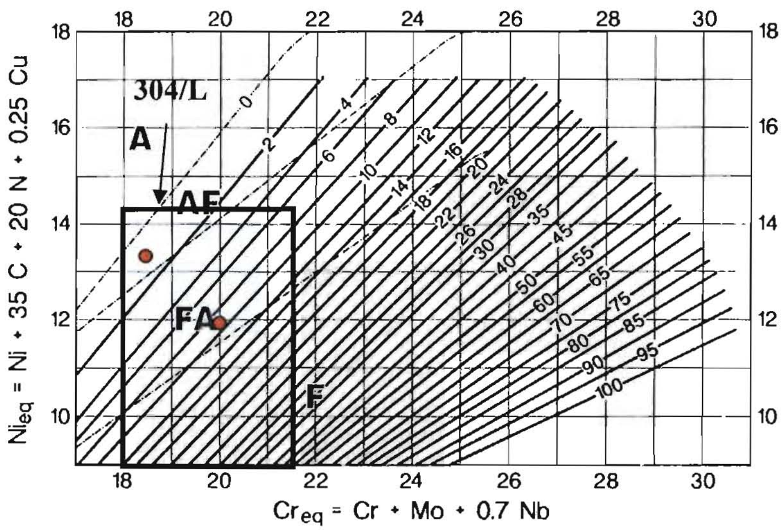

Fig. 11. WRC-1992 diagram [19] showing the range for 304/L stainless steel composition. The two points are shown for the composition of materials investigated in the current study.

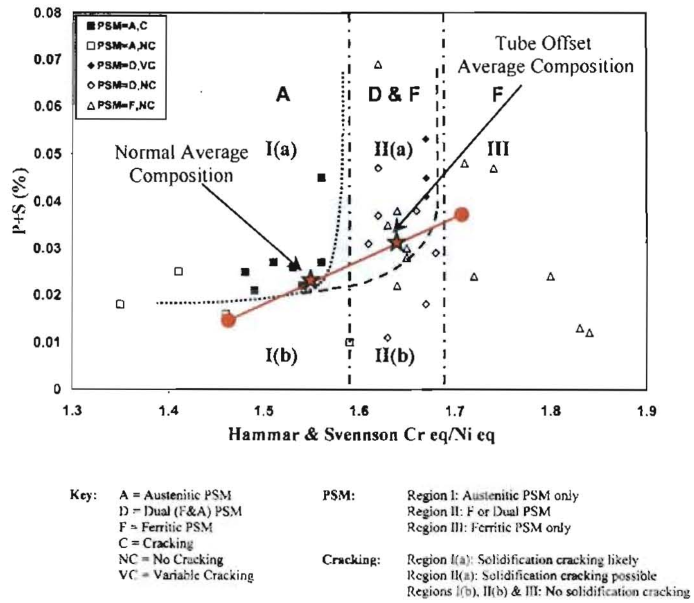

Fig. 12. Lienert/Lippold-modified weldability diagram [15] for pulsed laser beam welds. The end-points of the tie-lines indicate the material compositions, while the stars indicate the average composition based upon area fractions.

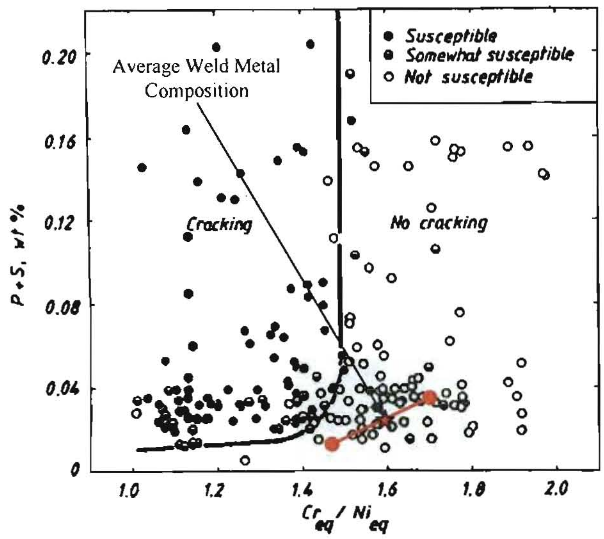

Fig. 13. Original weldability diagram [2] based upon GTAW with tie-line shown for current compositions.

A first order approximation of the cooling rate was shown first by Katayama and Matsunawa [25] and then used by Elmer, *et al.* [21]to be predicted by the following

$$\lambda_1 = 80(\varepsilon)^{-0.33} \qquad (1)$$

where λ_1 is the cell spacing (in μm) and ε is the cooling rate (in K/s). The cooling rate was not found to vary much between the lower power and higher power pulsed laser beam welds (*i.e.* conduction mode versus keyhole mode), all of which were estimated to be between 10^5 and 10^6 K/s. This observation is in good agreement with the predicted cooling rates reported in literature for pulsed laser welds [25,26]. Thus, it was determined that the cooling rate did not influence the observed change in solidification mode. Based upon the results of a previous investigation [24], the mixing was believed to have the greatest influence on the solidification mode *locally,* since the composition variations in the conduction mode weld allowed for a sizable unmixed zone and nonuniform mixing. The keyhole mode is a potent mode for vigorous mixing in the weld metal, as shown by the results of the previous investigation [24], and as such, allowed for a more uniform weld metal composition, which resulted in a more uniform weld metal microstructure. However, caution should be used in simply looking just at the composition and general cooling rate data. Zacharia, *et al.* [26] have shown that local variations in cooling rates are experienced at the different solidification fronts during pulsed laser welding, and different solidification modes and structures may result from these local variations.

Utilizing the approximation of cooling rate from the cell spacing for the pulsed GTA welded specimens, the cooling rate was estimated to be between 10^3 and 10^4 K/s.

Lippold [8] Elmer, *et al.* [21] and David *et al.* [20] have shown that a material that is predicted to have a PSM of ferrite-austenite may solidify as primary austenite at higher solidification rates. In fact, this was Lippold's premise when developing an understanding of why the cracking curve is shifted from the left to the right in the weldability diagram when employing high energy density welding processes [8].

Both Lippold [8] and Elmer, *et al.*, [21] have developed "solidification maps", which show expected primary solidification mode as a function of composition and some variable, such as solidification rate or welding travel speed. The current work utilizes Elmer's map, which shows PSM as a function of composition and EB scan speed, since the processes are both pulsed processes. Further, the EB scan speed related to cooling rate through Equation 1. Based upon this, the cooling rates were plotted as a range Elmer's diagram as an "Equivalent EB scan speed" and composition. Figure 14 shows Elmer's diagram with the pulsed LBW and pulsed GTAW ranges along with the composition ranges. It is easily seen from this figure that the PSM is predicted to be either fully A (pulsed LBW) or A/AF (pulsed GTAW). This map helps to explain why GTAW processing the dissimilar combination results in a weld metal susceptible to solidification cracking. This map does not fully explain the dual mode of primary solidification in the pulsed laser welded combination, and it was derived from 60% iron ternary alloys. Finally, even though the original weldability diagram (in Figure 12) was developed on GTAW, this work continues to emphasize that not all GTAW processes are equivalent – the solidification rates and resulting PSMs could be dramatically different depending upon the composition, the material dimensions and the welding parameters. Because of this, some caution should be used when employing the weldability diagrams available.

Finally, it should be noted that weld solidification cracking needs not only a crack-susceptible microstructure, but also sufficient tensile stress to drive a crack open. Certainly, a difference in stress between the conduction mode and keyhole mode exists. The resultant shape of the keyhole mode weld lends itself to higher resultant stress. In addition, both the pulsed LBW and pulsed GTAW processed materials showed both convex and concave weld profiles, which will certainly result in varied solidification stresses. The difference in stresses, however, was not quantified nor studied in this investigation.

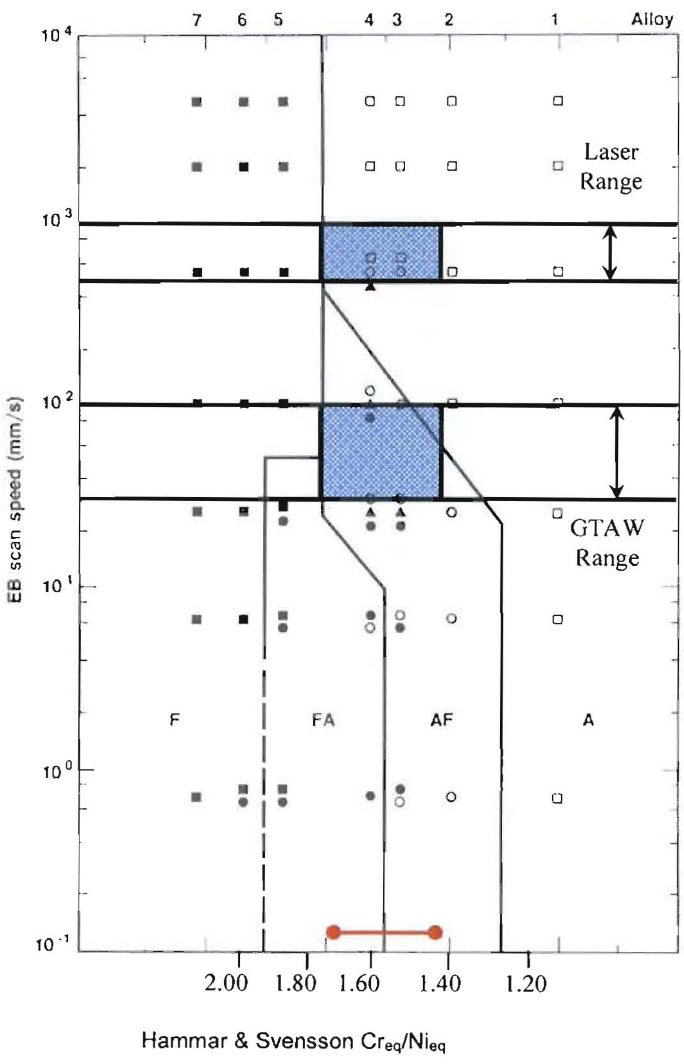

Fig. 14. Solidification mode map adapted from Elmer showing possible composition ranges of materials welded [21].

Conclusions

1. Welding similar materials that are "weldable" when welded autogenously may result in a weld metal that is susceptible to weld solidification cracking.
2. A modified weldability diagram with a tie-line between two compositions may be useful in predicting the susceptibility of the resulting weld metal to weld solidification cracking. This presumes that the weldability diagram used correlates to the applied welding conditions.
3. When utilizing the weldability diagrams, the user should verify that the diagram is applicable. For instance, even though the original weldability diagram was developed for GTAW processes, it is not applicable when the GTAW process is drastically different. This study showed that the original weldability diagram was not applicable for the pulsed GTA welds made for this investigation.

Acknowledgements

This work was funded under the auspices of the United States Department of Energy, Los Alamos National Laboratory, which is operated by the Los Alamos National Security, LLC for the National Nuclear Security Administration of the U.S. Department of Energy under contract DE-AC52-06NA25396. The authors would like to thank Dr. Paul Burgart and Mr. John Mileski for many useful discussions. The authors would also like to thank Dr. Mark Paffett for his timely and insightful review.

References

1. Arata, R.J., Matsuda, F., and Katayama, S., 1976. Fundamental Investigation on Solidification Behavior of Fully Austenitic and Duplex Structures and Effect of Ferrite on Microsegregation, *Transactions of JWRI*, 1976, pp. 35-51.
2. Kujanpää, V., Suutala, N., Takalo, T., and Moisio, T., 1979. Correlation Between Solidification Cracking and Microstructure in Austenitic and Austenitic-Ferritic Stainless Steel, *Welding Research International*, 1979, pp. 55-76.
3. Takalo, T., Suutala, N., and Moisio, T., 1979. Austenitic Solidification Mode in Austenitic Stainless Steel Welds, *Metallurgical Transactions A*, August 1979, pp. 1173-1181.

4. Suutala, N., Takalo, T., and Moisio, T., 1979. The Relationship Between Solidification and Microstructure in Austenitic and Austenitic-Ferritic Stainless Steel Welds, *Metallurgical Transactions A*, April 1979, pp. 512-514.
5. Suutala, N., Takalo, T., and Moisio, T., 1980. Ferritic-Austenitic Solidification Mode in Austenitic Stainless Steel Welds, *Metallurgical Transactions A*, May 1980, pp. 717-725.
6. Kujanpää, V., Suutala, N., Takalo, T., and Moisio, T., 1980. Solidification Cracking – Estimation of the Susceptibility of Austenitic and Austenitic-Ferritic Stainless Steel Welds, *Metal Construction*, June 1980, pp.282-285.
7. Suutala, N., 1983. Effect of Solidification Conditions on the Solidification Mode in Austenitic Stainless Steels, *Metallurgical Transactions A*, February, 1983, pp. 191-197.
8. Lippold, J.C., 1994. Solidification Behavior and Cracking Susceptibilty of Pulsed-Laser Welds in Austenitic Stainless Steel, *Welding Journal*, June, 1994, pp. 129-s - 139-s.
9. Hull, F.C., 1967. Effect of Delta Ferrite on Hot Cracking of Stainless Steel, *Welding Journal*, September 1967, pp. 399-s – 409-s.
10. Masumoto, I., Tamaki, K., and Kutsuna, M., 1972. Hot Cracking of Austenitic Stainless Steel Weld Metal, *Transactions of the Japan Welding Society*, 1972, pp. 1306-1314.
11. David, S.A., Goodwin, G.M., and Braski, D.N., 1979. Solidification Behavior of Austenitic Stainless Steel Filler Metals, *Welding Journal*, November 1979, pp. 330-s – 336-s.
12. Lippold, J.C., 1982. Weld Cracking Mechanism in Austenitic Stainless Steels, Proceedings from the Trends in Welding Research in the U.S., ASM Conference Proceedings, Materials Park, Ohio, 1982, pp.209-247.
13. Brooks, J.A. and Thompson, A.W., 1991. Micorstructural Development and Solidification Cracking Susceptibility of Austenitic Stainless Steel Welds, *International Materials Reviews*, 1991, pp. 16-44.
14. Brooks, J.A., Thompson, A.W., and Williams, J.C., 1984. A Fundamental Study of the Beneficial Effects of Delta Ferrite in Reducing Weld Cracking, *Welding Journal*, March 1984, pp. 71-s - 83-s.
15. Lienert, T.J., and Lippold, J.C., 2003, Improved Weldability Diagram for Pulsed Laser Welded Austenitic Stainless Steels, *Science and Technology of Welding and Joining*, January, 2003, pp. 1-9.
16. A.L. Schaeffler, A.L., 1949. Constitution Diagram for Stainless Steel Weld Metal, *Metal Progress*, 1949, pp. 680-680B.
17. DeLong, W.T., Ostrom, G.A., and Szumachowski, E.R., 1956. Measurement and Calculation of Ferrite in Stainless Steel Weld Metal, *Welding Journal*, November 1956, pp. 526-s – 33-s.
18. Siewert, T.A., McCowan, C.N., and Olson, D.L., 1988. Ferrite Number Prediction to 100 FN in Stainless Steel Weld Metal, *Welding Journal*, December 1988, pp. 289-s – 298-s.
19. Kotecki, D., and Siewert, T.A., 1992. WRC-1992 Constitution Diagram for Stainless Steel Weld Metals, *Welding Journal*, May 1992, pp. 171-s - 178-s.

20. David, S.A., Vitek, J.M., and Hebble, T.L., 1987. Effect of Rapid Solidification on Stainless Steel Weld Metal Microstructures and Its Implications on the Schaeffler Diagram, *Welding Journal*, October 1987, pp. 289-s - 300-s.
21. Elmer, J.W., Allen, S.M., and Eager, T.W., 1989. Microstructural Development During Solidification of Stainless Steel Alloys, *Metallurgical Transasctions A*, October, 1989, pp. 2117-2131.
22. Viteck, J.M., Dasgupta, A., and David, S.A., 1983. Microstructural Modification of Austenitic Stainless Steels by Rapid Solidification, *Metallurgical Transactions A*, September 1983, pp. 1833-1841.
23. Lippold, J.C., 1985. Centerline Cracking in Deep Penetration Electron Beam Welds in Type 304L Stainless Steel, *Welding Journal*, May 1985, pp 127-s - 136-s.
24. Hochanadel, P.W., Cola, M.J., Kelly, A.M., and Papin, P.A., 2002, Pulsed Laser Beam Welding of 304 to 304L Stainless Steel: Effects of Welding Parameters on Cracking and Phase Transformations, Proceedings of Joining of Advanced and Specialty Materials IV, Indianapolis, Indiana, 2001, publ. by ASM International, pp. 16-21.
25. Katayama, S. and Matsunawa, A., 1985. Solidification Microstructure of Laser Welded Stainless Steels, Proceedings of the Materials Processing Symposium -ICALEO '84, LIA-Laser Institute of America, Toledo, OH 1985 pp. 60-7
26. Zacharia, T., David, S.A., Vitek, J.M., and Debroy, T., 1989, Heat Transfer During Nd:YAG Pulsed Laser Welding and Its Effect On Solidification Structure of Austenitic Stainless Steels, *Metallurgical Transasctions A*, May 1989, pp. 957-967.